Report

Current Biology

Running performance in *Australopithecus afarensis*

Highlights

- Maximum running speed of *Australopithecus* was considerably lower than modern humans
- The submaximal (endurance) running speed range was limited in *Australopithecus*
- Energetics cost in *Australopithecus* was similar to other mammals and birds
- These results suggest the human body plan evolved for improved running performance

Authors

Karl T. Bates, Sian McCormack, Evie Donald, ..., Thomas O'Mahoney, Pasha A. van Bijlert, William I. Sellers

Correspondence

k.t.bates@liverpool.ac.uk

In brief

Bates et al. present the first physics simulations of running in *Australopithecus* and demonstrate that maximum running speed was considerably lower than modern humans, with a restricted submaximal range available for endurance running, which suggests that key features in the human body plan evolved specifically for improved running performance.

Bates et al., 2025, Current Biology *35*, 224–230
January 6, 2025
https://doi.org/10.1016/j.cub.2024.11.025

CellPress

CellPress
OPEN ACCESS

Current Biology

Report

Running performance in *Australopithecus afarensis*

Karl T. Bates,[1,8,9,*] Sian McCormack,[1,8] Evie Donald,[2] Samuel Coatham,[3] Charlotte A. Brassey,[4] James Charles,[1,8] Thomas O'Mahoney,[5] Pasha A. van Bijlert,[6,7] and William I. Sellers[3]

[1]Department of Musculoskeletal & Ageing Science, Institute of Life Course & Medical Sciences, University of Liverpool, The William Henry Duncan Building, 6 West Derby Street, Liverpool L7 8TX, UK
[2]School of Medicine, Faculty of Health Sciences and Wellbeing, University of Sunderland, Murray Health, Chester Road, Sunderland SR1 3SD, UK
[3]School of Natural Sciences, University of Manchester, Michael Smith Building, Oxford Road, Manchester M13 9PT, UK
[4]Department of Natural Sciences, Manchester Metropolitan University, Manchester M1 5GD, UK
[5]School of Life Sciences, Faculty of Science and Engineering, Anglia Ruskin University, Cambridge CB1 1PT, UK
[6]Department of Earth Sciences, Faculty of Geosciences, Utrecht University, Vening Meinesz Building A, Princetonlaan 8a, 3584 CB Utrecht, the Netherlands
[7]Naturalis Biodiversity Center, Darwinweg 2, 2333 CR Leiden, the Netherlands
[8]X (formerly Twitter): @LivEvoBiomech
[9]Lead contact
*Correspondence: k.t.bates@liverpool.ac.uk
https://doi.org/10.1016/j.cub.2024.11.025

SUMMARY

The evolution of bipedal gait is a key adaptive feature in hominids,[1–16] but the running abilities of early hominins have not been extensively studied.[2] Here, we present physics simulations of *Australopithecus afarensis* that demonstrate this genus was mechanically capable of bipedal running but with absolute and relative (size-normalized) maximum speeds considerably inferior to modern humans. Simulations predicted running energetics for *Australopithecus* that are generally consistent with values for mammals and birds of similar body size, therefore suggesting relatively low cost of transport across a limited speed range. Through model parameterization, we demonstrate the key role of ankle extensor muscle architecture (e.g., the Achilles tendon) in the evolution of hominin running energetics and indeed in an increase in speed range, which may have been intrinsically coupled with enhanced endurance running capacity. We show that skeletal strength was unlikely to have been a limiting factor in the evolution of enhanced running ability, which instead resulted from changes to muscle anatomy and particularly overall body proportions. These findings support the hypothesis that key features in the human body plan evolved specifically for improved running performance[2,3] and not merely as a byproduct of selection for enhanced walking capabilities.

RESULTS AND DISCUSSION

Overview of approach

The evolution of a low-cost bipedal gait is a key adaptive feature in hominins.[1–16] Due to its somewhat "intermediate" body plan and near-complete osteology, *Australopithecus afarensis* has often been identified as a key fossil taxon for understanding the evolution of bipedalism in our lineage[2,3,8–16] (Figure 1A). Analyses of fossilized skeletons[7,16] and footprints[8] have provided convincing evidence that australopithecines adopted mechanically efficient, upright ("human-like") bipedal walking gaits by at least 3.7 Ma. However, they retained relatively long arms and other features indicative of arboreality,[1,9–11] while lacking a number of evolutionary innovations considered fundamental to modern human bipedalism.[1–3,9–12] In their seminal work on the evolution of hominid running abilities, Bramble and Lieberman[2] (see also Carrier[3]) noted that major anatomical features of enhanced bipedal running performance were present in *H. erectus* but probably or definitely absent in australopithecines (Figure 1A, gray bars). This suggests a considerable shift in running performance at the evolution of *Homo*, although the nature of this shift is currently unclear.[2] As yet, the running abilities of early hominins like *Au. afarensis* have not been quantitatively estimated. This limits our understanding of the locomotor ecology of early hominins and, subsequently, our ability to interpret the nature of changes to locomotor mechanics and ecology within early *Homo* and the selective pressures that drove them.

Steady-state running performance has three major components: top speed (or the range of achievable speeds), energetic cost (often quantified as cost of transport [CoT]), and endurance capacity.[2,3,20] Here, we use dynamic gait simulations to estimate running performance in *Au. afarensis*, using the near-complete AL 288-1 ("Lucy") skeleton as a basis for our digital musculoskeletal model (Figure 1B). By subjecting this digital model to physics simulation and a machine learning optimization approach[7,8,21–23] we were able to directly assess maximal running speed (and the range of achievable speeds) and associated energetic costs in *Au. afarensis*, with the predictive accuracy of this approach demonstrated by the close match between our simulations of human running and experimental gait measurements, including maximum speed, spatiotemporal parameters, and peak vertical ground reaction forces (Figure S3), and to a lesser extent joint

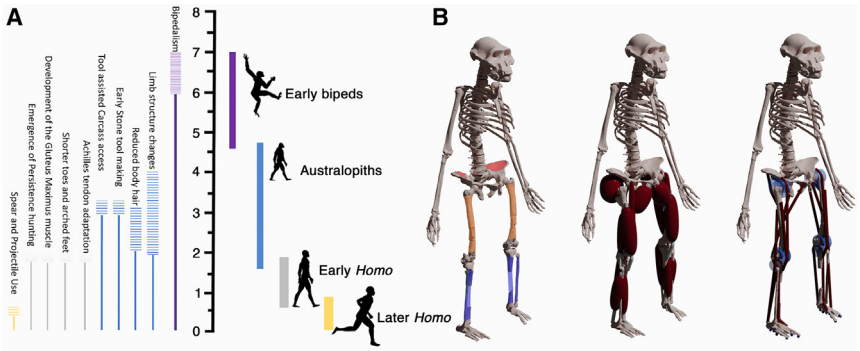

Figure 1. The evolution of locomotor anatomy and running performance in hominins

(A) Indicative timeline of major events related to the emergence of bipedalism and long-distance running.[17–19] Where dates are uncertain in the literature, the commonly accepted time frame is indicated by dashed lines.

(B) Reconstructing locomotor anatomy and running performance in *Au. afarensis* based on the AL 288-1 ("Lucy") fossil. The relationship between bone surface areas (left image) and muscle mass in extant apes and gibbons was used to predict the masses of major muscle groups in the lower limb of *Au. afarensis* (central image), which was combined with other data in a multi-body dynamics (MDA) model (right image). This MDA model was then combined with machine learning algorithms in a physics simulation environment to reconstruct optimal running gaits in *Au. afarensis*.

kinematics (Figure S4). Through model parameterization, we also assess how these performance metrics are impacted by specific anatomical adaptations that are considered key to the evolution of human running performance. Here, we focus on three key muscle-tendon traits: muscle mass, the architecture of the triceps surae muscles (including Achilles tendon development), and muscle contractile velocity.

Running speed and energetics in *Au. afarensis*

Our gait optimization simulations yielded steady-state running gaits with an aerial phase in *Au. afarensis* (Figures 2 and 3; see also Videos S1, S2, and S3). Notably, we even found true running gaits in models where muscle mass was lowered to the same relative values as chimpanzees and triceps surae architecture was represented by an extreme non-human ape-like morphology (Figure 3; Video S2), with Achilles tendon length reduced by more than 80% and physiological cross-sectional areas by more than 60% (as a consequence of much longer muscle fiber lengths) in the two ankle extensor muscles. This provides quantitative evidence that the australopithecine body plan was capable of true steady-state bipedal running gaits, even if major hallmarks of modern human running were absent. However, maximum running speed was considerably lower than our human model (7.9 m/s) across all our different model iterations, with absolute speeds ranging from 1.74 to 4.97 m/s (Figure 3; Table S2). This speed range was defined by model iterations with modern human muscle mass proportions and triceps surae architecture and model iterations with chimpanzee muscle mass proportions and extreme non-human ape triceps surae architecture. Speeds predicted where maximum contraction velocity was altered to values well above and below those typically used in human models fell within this range (Figure 3). After size-normalization to remove the effects of body size (through calculation of Froude numbers [Fr]) running speed remained considerably lower in *Au. afarensis* (Fr = 0.56–4.57) compared with our human model (Fr = 7).

Some simulation iterations of the *Au. afarensis* model with non-human ape triceps surae architecture failed to optimize to true aerial running gaits, which means that collectively our simulations capture the walk-run transition and thus the lower and upper bounds of running speeds (Figure 3; Table S2). The slowest iteration achieved a speed of 1.17 m/s (Fr = 0.25) with a duty factor of 0.61 and thus exhibits an unequivocal walking gait, while a simulation with an average speed of 1.42 m/s (Fr = 0.38) had a duty factor of 0.503 (Figure 3; Table S2). Capturing this walk-run transition highlights the limited absolute and relative range of running speeds (~1.5–4.97 m/s, Fr = ~0.4–4.57) in *Au. afarensis* compared with modern humans, particularly if more human-like muscle proportions and architecture were not present (~1.42–2.28 m/s, Fr = ~0.4–0.97).

Despite much lower relative and absolute speeds, metabolic CoT was between 1.7 and 2.9 times higher across these different *Au. afarensis* model iterations than in the human model (Figure 3; Table S2). However, CoT in running is known to scale with negatively allometry in mammals and birds.[24,25] In other words, smaller animals inherently use more energy to travel a given distance than larger animals when body size is accounted for (Figure 4). Examination of our predicted running energetics for *Au. afarensis* in this wider allometric context[24,25] suggests that our model with modern human triceps surae architecture yields values for CoT that fall within the range of values seen in living mammals and birds of a similar body size and, in some cases, close the predicted average values (Figure 4). Therefore, the greater CoT predicted for *Au. afarensis* relative to modern humans (Figure 3) may be largely, if not completely, explained by body size alone if *Au. afarensis* possessed human-like triceps surae architecture (Figure 4). However, model iterations with non-human ape triceps surae architecture (i.e., relatively longer muscle fibers and little Achilles tendon) have slightly higher CoTs than would be predicted based on the allometric relationship seen in extant mammals and birds[24,25] (Figure 4). Viewing energetic predictions in this wider context therefore emphasizes the crucial role of the Achilles tendon and triceps surae architecture in the evolution of hominin running energetics.

Skeletal stress and running performance

Bramble and Lieberman[2] cited skeletal strength as one of the structural bases underpinning the evolution of human running performance, noting that australopithecines have robust femoral shafts relative to body mass that are narrower transversely than in early *Homo*, suggesting that changes to bone geometry may have been necessary to sustain the higher forces associated with enhanced running ability.[2,26,27] Research on limb bone safety factors in cursorial vertebrates during running and other high-performance activities suggests that these elements typically experience maximum stress of around 100 MPa,[28,29]

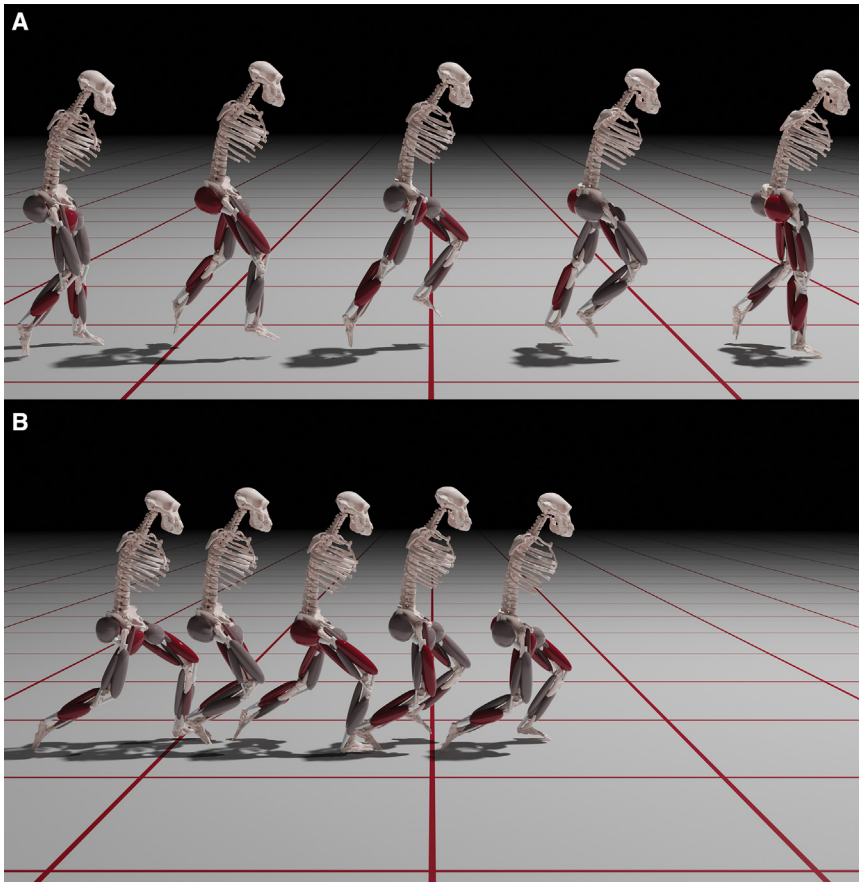

Figure 2. Simulating running performance in *Au. afarensis*

(A and B) Snapshots of the fastest running gait predicted for *Au. afarensis* where triceps surae architecture was modeled with (A) human-like and (B) an "extreme" non-human ape (NHA) morphology (i.e., very long muscle fibers but a very small Achilles tendon). Both sequences in (A) and (B) show 0.65 s of simulation time, demonstrating the greater distance traveled in the model with human-like triceps surae architecture (see also Videos S1, S2, and S3). Active muscles are dark red, inactive muscles are gray. The overall size of muscle volumes is consistent with those predicted here for *Au. afarensis*, but their shape was subjectively specified to allow visualization of muscle paths.

leading to the suggestion that cursorial vertebrates typically exhibit safety factors of 2–4 in their limb bones.[28–30]

Using cross-sectional geometries from the AL 288-1 fossil[31] and the volunteer upon which our human model was based,[32,33] we calculated the bone stress incurred in our running simulations by treating the limb long bones as irregular beams and calculating the mid-shaft loading.[23] The highest stresses recovered across all our *Au. afarensis* simulations equated to peak compressive stresses at midshaft in the femur and shank of −32 and −30 MPa and peak bending stresses of 33 and 27 MPa (Table S3), which equate to generous safety factors of at least 5–6. Indeed, there are perhaps reasons to believe that our models may overestimate midshaft stress at these simulated speeds because viscoelasticity of bone tissue and ligament elasticity would attenuate locomotor impacts if we were to incorporate them in our model. While studies have shown higher muscle activations in other demanding locomotor tasks (e.g., maximal jumping[34]) that might potentially lead to higher skeletal loads, our results nevertheless suggest that changes to body proportions and limb muscles (Figure 3) were considerably more important than skeletal strength to the early evolution of enhanced running ability in hominins, at least in terms of limb bone midshaft loading. Expanded limb bone joint surface area is also cited as a key adaptation in humans to enhance running performance.[2] Future work could use our simulation outputs in additional types of mechanical analyses, such as finite element models, to quantify changes in joint surface loading in hominins.

Evolutionary perspectives and key innovations in running performance

For the first time, we have directly estimated running ability in *Au. afarensis* using musculoskeletal modeling and physics simulation. Systematic manipulation of the muscular anatomy of the *Au. afarensis* and human models allows us to isolate the impact of key anatomical traits on hominin running performance. Humans possess a long spring-like Achilles tendon connecting short-fibered ankle extensor muscles to the calcaneus.[31,33,31–33] This combination of short fibers and a well-developed Achilles tendon facilitates more economical force generation, power amplification, and ultimately a reduction in locomotor cost through storage and return of elastic energy.[35–38] Our simulations emphasize that differences in the architecture of the triceps surae (ankle extensor) muscles in extant non-human apes and humans are crucial to their vastly different bipedal running performance (Figures 3 and 4; Video S3). For example, in *Au. afarensis* models using our predicted muscle masses based on skeletal attachment areas, maximum speed and CoT were 4.26 m/s and 5.21 J/kg/m with human-like triceps surae architecture (Figure 3; Video S1), compared with 2.28 m/s and 7.42 J/kg/m with non-human ape triceps surae architecture (Figure 3; Video S2). Maximum speed with non-human ape triceps surae architecture was therefore only 54% that achieved with human-like triceps surae architecture, while CoT was 42% higher. In the human model, the effects were also relatively large, with a switch to non-human ape-like triceps surae architecture reducing maximum speed to 59% of that achieved by the normal human model while increasing CoT by around 88% of the normal model's predicted value (Figure 3).

Interestingly, the considerable increase in CoT incurred in both human and *Au. afarensis* models with non-human ape triceps surae architecture does not appear to be solely the product of changes in metabolic power, work, and energy storage in the triceps surae (ankle extensor) muscles themselves (Figures S4E and S4F). While energy storage in ankle extensor serial elements is noticeably lower in these model iterations (Figure S4F), it is

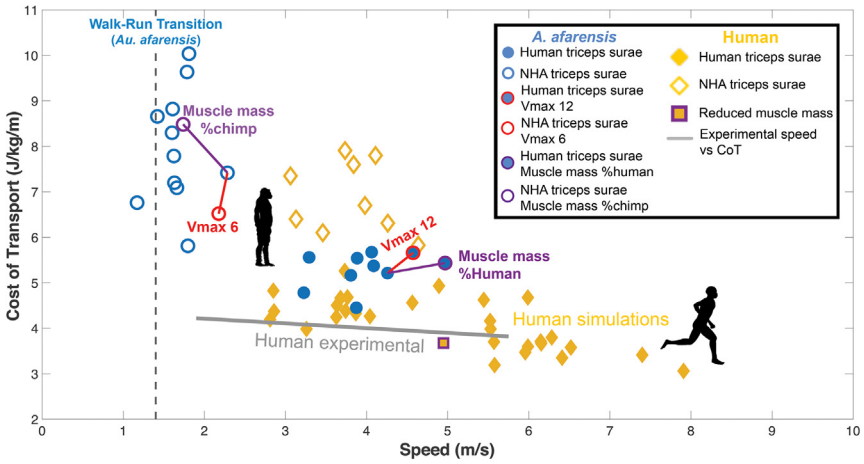

Figure 3. Comparison of CoT and absolute running speed from all optimized iterations of the *Au. afarensis* and human models

Simulations of both human and *Au. afarensis* models where triceps surae architecture was modeled as an "extreme" non-human ape morphology (open data points) yielded slower maximum speeds and higher CoTs than models with human-like triceps surae architecture (i.e., shorter muscle fibers and a well-developed Achilles tendon). The fastest *Au. afarensis* simulation with human-like triceps surae architecture was tested with increased muscle mass (blue circle with purple outline) and higher $V_{max.}$ (blue circle with red outline) to provide an upper bound on predicted maximum speed, while the fastest *Au. afarensis* simulation with non-human ape-like triceps surae architecture was tested with decreased muscle mass (circle with purple outline) and lower $V_{max.}$ (circle with red outline) to provide a lower bound on predicted maximum speed.

clear that additional changes to limb kinematics and the contractile dynamics of other muscles are also contributing to the increased CoTs. In particular, both human and *Au. afarensis* simulations with non-human ape triceps surae architecture adopt more flexed limb joint postures, particularly at the knee (Figure S4C). Flexed limb postures incur reduced effective mechanical advantages through increased ground reaction force moments and lower muscle moment arms,[28,39] and, in our models, this leads to considerable increase in the metabolic work from the knee extensors (Figure S4E).

These manipulations of hominin anatomy illustrate that increased muscle mass and particularly triceps surae architecture may potentially, by themselves, account for evolutionary significant decreases in the metabolic CoT of running in the human ancestral lineage (Figure 4). However, our simulations suggest that these factors alone cannot account for higher relative and absolute speeds in our human model compared with *Au. afarensis* (Figure 3; Video S3). Specifically, even if *Au. afarensis* had human-like muscle mass and triceps surae architecture (Fr = 4.57, 4.97 m/s), its top speed would still be substantially slower in both relative and absolute terms than that of a non-elite athlete modern human (Fr = 7, 7.9 m/s). Our simulations suggest *Au. afarensis* with modern human-like muscles would be similar in absolute speeds (and therefore slightly higher in relative terms) to our hypothetical human model in which these muscular adaptations have been removed (lower muscle mass model Fr = 2.74, 4.94 m/s; non-human ape triceps surae architecture model Fr = 2.41, 4.64 m/s; Figure 3). With muscle-tendon anatomy manipulated in these model iterations, the major outstanding difference between the models of *Au. afarensis* and the modern human is their relative body proportions. The fact that human-like muscle masses and architectures in our *Au. afarensis* model yield broadly similar speeds to the human model iterations with compromised muscle morphologies therefore suggests that the australopithecine body plan, with its relatively larger upper body and arms and shorter legs, significantly limited maximum running speed (Figure 3), but may not have significantly limited running energetics (Figure 4). Indeed, these differences in body proportions are thought to be coupled with additional dynamic factors[2] that are not included in our simplified models (e.g., arm swing, torso rotations: see STAR Methods for additional discussion), which may further exaggerate differences in locomotor performance between australopithecines and *Homo*.

Endurance running capacity is considered a central factor in the evolution of human locomotion.[2,3,20] Locomotor endurance has been defined as the maximum amount of time that an individual can sustain a given speed[24] and is ultimately thought to be governed by physiological "fatigue" factors, such as muscle oxygenation and lactate production.[40] To our knowledge, no whole-body gait simulation approach like ours has yet incorporated true cumulative physiological fatigue, and thus our ability to directly assess long-distance endurance capacity through predictive musculoskeletal modeling is currently limited. However, our simulations may provide some important indirect insights into the relative endurance running capabilities of australopithecines and humans. In particular, we find that even if relatively large human-like limb muscle masses and triceps surae architecture were present in *Au. afarensis*, it would have a considerably narrower range of running speeds relative to modern humans (~1.5–4.97 m/s, Fr = ~0.4–4.57). This running speed range is constricted further in the absence of human-like muscle masses and architectures (~1.42–2.28 m/s, Fr = ~0.4–0.97). Furthermore, at higher ("sprint") speeds (e.g., above ~6 m/s in humans[2,3,30]) animals switch to anaerobic respiration and typically are unable to carry out sustained or endurance running. By ruling out the highest speeds, this effectively further constricts the range of predicted running speeds (Figure 3) potentially available to *Au. afarensis* to perform endurance running. This raises the possibility that endurance capacity and top speed were intrinsically coupled in the evolution of running, both mechanistically in terms of musculoskeletal adaptations and ecologically through an increase in total running speed range. In other words, increased maximum running speed and thus speed range afforded by muscular adaptations (Figure 3) and human body proportions opened up much broader bounds of submaximal running speeds that could be exploited for long-distance locomotor bouts.

While some variation in body proportions exists within australopithecines,[12,13] an essentially modern human body shape probably appeared in the earliest members of the genus *Homo*, and

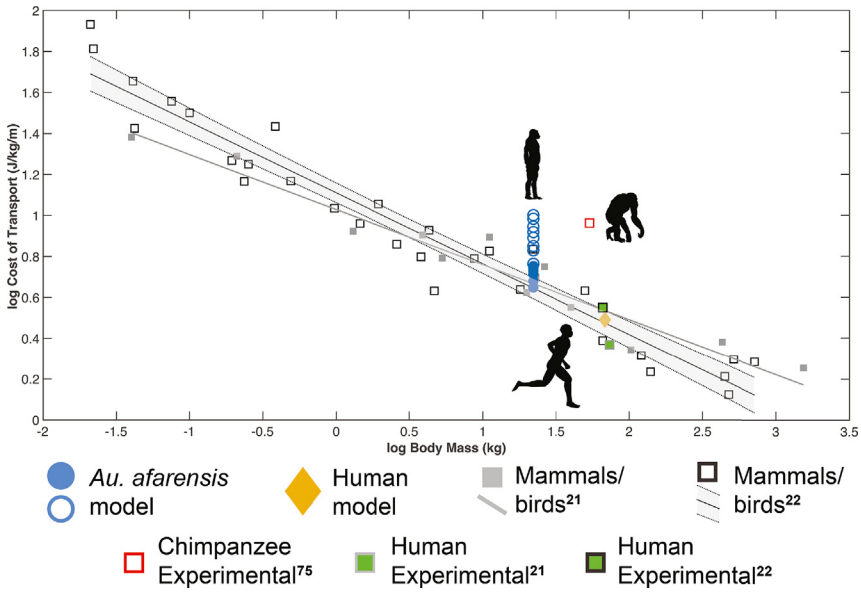

Figure 4. Scaling of metabolic CoT in mammals and birds

Our predicted CoTs for running in *Au. afarensis* fall within the experimentally measured range and are close to or below scaling predictions for a 22 kg terrestrial mammal/bird based on data from Pontzer[24] and Rubenson et al.[21] Model iterations with human triceps surae architecture (i.e., relatively short muscle fibers and a well-developed Achilles tendon) have CoTs that are slightly lower than dogs and goats of a similar body mass. Model iterations with an "extreme" non-human ape (NHA) triceps surae architecture (i.e., relatively long muscle fibers and little Achilles tendon) have higher CoTs that deviate further from values that would be predicted for a 22 kg mammal or bird.[24,25] The shaded area within the dashed lines denotes the upper and lower 95% confidence intervals about the best-fit line of Rubenson et al.[25]

certainly in *H. erectus* by 1.8 Ma.[1,2,9,10] Some researchers have suggested that walking economy or bipedalism generally was the major driver behind the evolution of postcranial proportions, while others have linked the appearance of modern human body shape and its associated skeletal features specifically with enhanced running performance.[2,3,41–46] It is now widely accepted that australopithecines used broadly human-like extended (upright) walking gaits,[7,8,10,14] but our results demonstrate disparate running performance. In particular, we find that human body proportions are associated with higher absolute and relative maximum speeds and, as a byproduct, a considerably extended submaximal running speed range that can be exploited for endurance running bouts (Figure 3). This finding suggests that key features in the human body plan evolved specifically for improved running performance[2,3] and not merely as a byproduct of selection for enhanced walking capabilities.

RESOURCE AVAILABILITY

Lead contact

Requests for resources or further information should be directed to the lead contact, Karl T. Bates (k.t.bates@liverpool.ac.uk).

Materials availability

See the key resources table for materials used in this study.

Data and code availability

The multi-body dynamics models of the human and *Au. afarensis* have been deposited at the University of Liverpool's DataCat repository (https://doi.org/10.17638/datacat.liverpool.ac.uk/2831) and are publicly available as of the date of publication.

This paper does not report original code, but the GaitSym software required to visualize the MDA models is available at http://github.com/wol101.

Any additional information required to reanalyze the data reported in this paper is available from the lead contact upon request.

ACKNOWLEDGMENTS

Simulation work was undertaken on Barkla, part of the High-Performance Computing facilities at the University of Liverpool (UK), and Cliff Addison and Manhui Wang are thanked for their assistance using the system. This work was funded by grants from the Leverhulme Trust (RPG-2017-296), the Natural Environment Research Council (NE/C520447/1, NE/C520463/1, and NE/S00713X/1), and a Palaeontological Association Undergraduate Research Bursary (PA-UB202001).

AUTHOR CONTRIBUTIONS

K.T.B., W.I.S., C.A.B., and T.O. conceived the study. K.T.B., S.M., and W.I.S. designed the study. K.T.B., S.M., E.D., J.C., C.A.B., and T.O. collected the data. K.T.B., S.M., E.D., J.C., S.C., and P.V.B. processed the data. K.T.B. and P.V.B. analyzed the data. All authors contributed to the manuscript.

DECLARATION OF INTERESTS

The authors declare no competing interests.

STAR★METHODS

Detailed methods are provided in the online version of this paper and include the following:

- KEY RESOURCES TABLE
- EXPERIMENTAL MODEL AND STUDY PARTICIPANT DETAILS
- METHOD DETAILS
  - Predicting muscle mass in *Australopithecus afarensis*
  - Body segment mass and inertial properties in *Australopithecus afarensis*
  - Simulating running performance
- QUANTIFICATION AND STATISTICAL ANALYSIS

SUPPLEMENTAL INFORMATION

Supplemental information can be found online at https://doi.org/10.1016/j.cub.2024.11.025.

Received: July 26, 2024
Revised: October 10, 2024
Accepted: November 14, 2024
Published: December 18, 2024

REFERENCES

1. Thorpe, S.K.S., Holder, R.L., and Crompton, R.H. (2007). Origin of human bipedalism as an adaptation for locomotion on flexible branches. Science *316*, 1328–1331.
2. Bramble, D.M., and Lieberman, D.E. (2004). Endurance running and the evolution of *Homo*. Nature *432*, 345–352.
3. Carrier, D.R., Kapoor, A.K., Kimura, T., Nickels, M.K., Scott, E.C., So, J.K., and Trinkaus, E. (1984). The energetic paradox of human running and hominid evolution [and Comments and Reply]. Curr. Anthropol. *25*, 483–495.
4. Haile-Selassie, Y. (2001). Late Miocene hominids from the Middle Awash, Ethiopia. Nature *412*, 178–181.
5. Spoor, F., Wood, B., and Zonneveld, F. (1994). Implications of early hominid labyrinthine morphology for evolution of human bipedal locomotion. Nature *369*, 645–648.
6. Brunet, M., Guy, F., Pilbeam, D., Mackaye, H.T., Likius, A., Ahounta, D., Beauvilain, A., Blondel, C., Bocherens, H., Boisserie, J.R., et al. (2002). A new hominid from the Upper Miocene of Chad, Central Africa. Nature *418*, 145–151.
7. Sellers, W.I., Cain, G.M., Wang, W., and Crompton, R.H. (2005). Stride lengths, speed and energy costs in walking of *Australopithecus afarensis*: using evolutionary robotics to predict locomotion of early human ancestors. J. R. Soc. Interface *2*, 431–441.
8. Crompton, R.H., Pataky, T.C., Savage, R., D'Août, K., Bennett, M.R., Day, M.H., Bates, K.T., Morse, S., and Sellers, W.I. (2012). Human-like external function of the foot, and fully upright gait, confirmed in the 3.66 million year old Laetoli hominin footprints by topographic statistics, experimental footprint-formation and computer simulation. J. R. Soc. Interface *9*, 707–719.
9. Stern, J.T., and Susman, R.L. (1983). The locomotor anatomy of *Australopithecus afarensis*. Am. J. Phys. Anthropol. *60*, 279–317.
10. Crompton, R.H., Vereecke, E.E., and Thorpe, S.K.S. (2008). Locomotion and posture from the common hominoid ancestor to fully modern hominins, with special reference to the last common panin/hominin ancestor. J. Anat. *212*, 501–543.
11. Ward, C. (2002). Interpreting the posture and locomotion of *Australopithecus afarensis*: where do we stand? Am. J. Phys. Anthropol. *119*, 185–215.
12. Haile-Selassie, Y., Latimer, B.M., Alene, M., Deino, A.L., Gibert, L., Melillo, S.M., Saylor, B.Z., Scott, G.R., and Lovejoy, C.O. (2010). An early *Australopithecus afarensis* 919 postcranium from Woranso-Mille, Ethiopia. Proc. Natl. Acad. Sci. USA *107*, 12121–12126.
13. Heaton, J.L., Pickering, T.R., Carlson, K.J., Crompton, R.H., Jashashvili, T., Beaudet, A., Bruxelles, L., Kuman, K., Heile, A.J., Stratford, D., et al. (2019). The long limb bones of the StW 573 *Australopithecus* skeleton from Sterkfontein Member 2: Descriptions and proportions. J. Hum. Evol. *133*, 167–197.
14. Wiseman, A.L.A. (2023). Three-dimensional volumetric muscle reconstruction of the *Australopithecus afarensis* pelvis and limb, with estimations of limb leverage. R. Soc. Open Sci. *10*, 230356.
15. O'Neill, M.C., Nagano, A., and Umberger, B.R. (2024). A three-dimensional musculoskeletal model of the pelvis and lower limb of *Australopithecus afarensis*. Am. J. Biol. Anthropol. *183*, e24845.
16. Nagano, A., Umberger, B.R., Marzke, M.W., and Gerritsen, K.G.M. (2005). Neuromusculoskeletal computer modeling and simulation of upright, straight-legged, bipedal locomotion of *Australopithecus afarensis* (A.L. 288-1). Am. J. Phys. Anthropol. *126*, 2–13.
17. McPherron, S.P., Alemseged, Z., Marean, C.W., Wynn, J.G., Reed, D., Geraads, D., Bobe, R., and Béarat, H.A. (2010). Evidence for stone-tool-assisted consumption of animal tissues before 3.39 million years ago at Dikika, Ethiopia. Nature *466*, 857–860.
18. Conard, N.J., Serangeli, J., Bigga, G., and Rots, V. (2020). A 300,000-year-old throwing stick from Schöningen, northern Germany, documents the evolution of human hunting. Nat. Ecol. Evol. *4*, 690–693.
19. Milks, A., Parker, D., and Pope, M. (2019). External ballistics of Pleistocene hand-thrown spears: experimental performance data and implications for human evolution. Sci. Rep. *9*, 820.
20. Pontzer, H. (2017). Economy and endurance in Human Evolution. Curr. Biol. *27*, R613–R621.
21. Sellers, W.I., and Manning, P.L. (2007). Estimating dinosaur maximum running speeds using evolutionary robotics. Proc. Biol. Sci. *274*, 2711–2716.
22. Bates, K.T., Manning, P.L., Margetts, L., and Sellers, W.I. (2010). Sensitivity analysis in evolutionary robotic simulations of bipedal dinosaur running. J. Vertebr. Paleontol. *30*, 458–466.
23. Sellers, W.I., Pond, S.B., Brassey, C.A., Manning, P.L., and Bates, K.T. (2017). Investigating the running abilities of *Tyrannosaurus rex* using stress-constrained multibody dynamic analysis. PeerJ *5*, e3420. https://doi.org/10.7717/peerj.3420.
24. Pontzer, H. (2007). Effective limb length and the scaling of locomotor cost in terrestrial animals. J. Exp. Biol. *210*, 1752–1761.
25. Rubenson, J., Heliams, D.B., Maloney, S.K., Withers, P.C., Lloyd, D.G., and Fournier, P.A. (2007). Reappraisal of the comparative cost of human locomotion using gait-specific allometric analyses. J. Exp. Biol. *210*, 3513–3524.
26. Jungers, W.L. (1988). Relative joint size and hominoid locomotor adaptations with implications for the evolution of hominid bipedalism. J. Hum. Evol. *17*, 247–265.
27. Ruff, C.B. (1998). Evolution of the hominin hip. In Primate Locomotion: Recent Advances, E. Strasser, J.G. Fleagle, A.L. Rosenberger, and H.M. McHenry, eds. (Plenum), pp. 449–469.
28. Biewener, A.A. (1989). Scaling body support in mammals: limb posture and muscle mechanics. Science *245*, 45–48.
29. Biewener, A.A. (1990). Biomechanics of mammalian terrestrial locomotion. Science *250*, 1097–1103.
30. Currey, J.D. (2000). Bones: Structure and Mechanics (Princeton University Press).
31. Ruff, C.B., Burgess, M.L., Ketcham, R.A., and Kappelman, J. (2016). Limb bone structural proportions and locomotor behavior in A.L. 288–1 ("Lucy"). PLoS One *11*, e0166095.
32. Charles, J.P., Grant, B., D'Août, K., and Bates, K.T. (2020). Subject-specific muscle properties from diffusion tensor imaging significantly improve the accuracy of musculoskeletal models. J. Anat. *237*, 941–959.
33. Charles, J.P., Kissane, R., Hoehfurtner, T., and Bates, K.T. (2022). From fibre to function: are we accurately representing muscle architecture and performance? Biol. Rev. Camb. Philos. Soc. *97*, 1640–1676.
34. Carrier, D.R., Schilling, N., and Anders, C. (2015). Muscle activation during maximal effort tasks: evidence of the selective forces that shaped the musculoskeletal system of humans. Biol. Open *4*, 1635–1642.
35. Ker, R.F., Bennett, M.B., Bibby, S.R., Kester, R.C., and Alexander, R.M. (1987). The spring in the arch of the human foot. Nature *325*, 147–149.
36. Kelly, L.A., Lichtwark, G., and Cresswell, A.G. (2015). Active regulation of longitudinal arch compression and recoil during walking and running. J. R. Soc. Interface *12*, 20141076.
37. Daley, M.A., and Biewener, A.A. (2003). Muscle force-length dynamics during level versus incline locomotion: a comparison of in vivo performance of two guinea fowl ankle extensors. J. Exp. Biol. *206*, 2941–2958.
38. Roberts, T.J., Marsh, R.L., Weyand, P.G., and Taylor, C.R. (1997). Muscular Force in Running Turkeys: The Economy of Minimizing Work. Science *275*, 1113–1115.
39. van Bijlert, P.A., van Soest, A.J., Schulp, A.S., and Bates, K.T. (2024). Muscle-controlled physics simulations of bird locomotion resolve the grounded running paradox. Sci. Adv. *10*, eado0936. https://doi.org/10.1126/sciadv.ado0936.
40. Noakes, T.D. (2011). Time to move beyond a brainless exercise physiology: the evidence for complex regulation of human exercise performance. Appl. Physiol. Nutr. Metab. *36*, 23–35.

41. Holowka, N.B., and Lieberman, D.E. (2018). Rethinking the evolution of the human foot: insights from experimental research. J. Exp. Biol. *221*, jeb174425.
42. Steudel-Numbers, K.L., and Wall-Scheffler, C.M. (2009). Optimal running speed and the evolution of hominin hunting strategies. J. Hum. Evol. *56*, 355–360.
43. Kramer, P.A. (1999). Modelling the locomotor energetics of extinct hominids. J. Exp. Biol. *202*, 2807–2818.
44. Kramer, P.A., and Eck, G.G. (2000). Locomotor energetics and leg length in hominid bipedality. J. Hum. Evol. *38*, 651–666.
45. Cunningham, C.B., Schilling, N., Anders, C., and Carrier, D.R. (2010). The influence of foot posture on the cost of transport in humans. J. Exp. Biol. *213*, 790–797.
46. Foley, R.A., and Elton, S. (1998). Time and energy: The ecological context for the evolution of bipedalism. In Primate Locomotion: Recent Advances, E. Strasser, J. Fleagle, A. Rosenberger, and H. McHenry, eds. (Plenum Press), pp. 419–433.
47. Sellers, W.I., Cross, C.F., Fukuhara, A., Ishiguro, A., and Hirasaki, E. (2022). Producing non-steady-state gaits (starting, stopping, and turning) in a biologically realistic quadrupedal simulation. Front. Ecol. Evol. *10*. https://doi.org/10.3389/fevo.2022.954838.
48. Püschel, T.A., and Sellers, W.I. (2016). Standing on the shoulders of apes: Analyzing the form and function of the hominoid scapula using geometric morphometrics and finite element analysis. Am. J. Phys. Anthropol. *159*, 325–341.
49. Brassey, C.A., O'Mahoney, T.G., Chamberlain, A.T., and Sellers, W.I. (2018). A volumetric technique for fossil body mass estimation applied to *Australopithecus afarensis*. J. Hum. Evol. *115*, 47–64.
50. Payne, R.C., Crompton, R.H., Isler, K., Savage, R., Vereecke, E.E., Günther, M.M., Thorpe, S.K., and D'Août, K. (2006). Morphological analysis of the hindlimb in apes and humans. I. Muscle architecture. J. Anat. *208*, 709–724.
51. Myatt, J.P., Crompton, R.H., and Thorpe, S.K.S. (2011). Hindlimb muscle architecture in non-human great apes and a comparison of methods for analysing inter-species variation. J. Anat. *219*, 150–166.
52. Thorpe, S.K.S., Crompton, R.H., Günther, M.M., Ker, R.F., and McNeill Alexander, R.M. (1999). Dimensions and moment arms of the hind- and forelimb muscles of common chimpanzees (*Pan troglodytes*). Am. J. Phys. Anthropol. *110*, 179–199.
53. Cuff, A.R., Wiseman, A.L.A., Bishop, P.J., Michel, K.B., Gaignet, R., and Hutchinson, J.R. (2023). Anatomically grounded estimation of hindlimb muscle sizes in Archosauria. J. Anat. *242*, 289–311.
54. Coatham, S.J., Sellers, W.I., and Püschel, T.A. (2021). Convex hull estimation of mammalian body segment parameters. R. Soc. Open Sci. *8*, 210836.
55. Sellers, W.I., Hepworth-Bell, J., Falkingham, P.L., Bates, K.T., Brassey, C.A., Egerton, V.M., and Manning, P.L. (2012). Minimum convex hull mass estimations of complete mounted skeletons. Biol. Lett. *8*, 842–845.
56. Macaulay, S., Hoehfurtner, T., Cross, S.R.R., Marek, R.D., Hutchinson, J.R., Schachner, E.R., Maher, A.E., and Bates, K.T. (2023). Decoupling body shape and mass distribution in birds and their dinosaurian ancestors. Nat. Commun. *14*, 1575. https://doi.org/10.1038/s41467-023-37317-y.
57. Minetti, A.E., and Alexander, R.M. (1997). A theory of metabolic costs for bipedal gaits. J. Theor. Biol. *186*, 467–476.
58. Ma, S.P., and Zahalak, G.I. (1991). A distribution-moment model of energetics in skeletal muscle. J. Biomech. *24*, 21–35.
59. Zajac, F.E. (1989). Muscle and tendon: properties, models, scaling, and application to biomechanics and motor control. Crit. Rev. Biomed. Eng. *17*, 359–411.
60. Carlson, K.J. (2006). Muscle architecture of the common Chimpanzee (*Pan troglodytes*): perspectives for investigating chimpanzee behavior. Primates *47*, 218–229.
61. O'Neill, M.C., Lee, L.F., Larson, S.G., Demes, B., Stern, J.T., and Umberger, B.R. (2013). A three-dimensional musculoskeletal model of the chimpanzee (*Pan troglodytes*) pelvis and hind limb. J. Exp. Biol. *216*, 3709–3723.
62. Myatt, J.P., Schilling, N., and Thorpe, S.K.S. (2011). Distribution patterns of fibre types in the triceps surae muscle group of chimpanzees and orangutans. J. Anat. *218*, 402–412.
63. O'Neill, M.C., Umberger, B.R., Holowka, N.B., Larson, S.G., and Reiser, P.J. (2017). Chimpanzee super strength and human skeletal muscle evolution. Proc. Natl. Acad. Sci. USA *114*, 7343–7348.
64. Umberger, B.R., Gerritsen, K.G.M., and Martin, P.E. (2003). A model of human muscle energy expenditure. Comput. Methods Biomech. Biomed. Engin. *6*, 99–111.
65. Alexander, R.M. (1976). Estimates of speeds of dinosaurs. Nature *261*, 129–130.
66. Mattes, K., Habermann, N., Schaffert, N., and Mühlbach, T.A. (2014). A longitudinal study of kinematic stride characteristics in maximal sprint running. J. Hum. Sport Exer. *9*, 686–699.
67. Brughelli, M., Cronin, J., and Chaouachi, A. (2011). Effects of running velocity on running kinetics and kinematics. J. Strength Cond. Res. *25*, 933–939.
68. Alcaraz, P.E., Palao, J.M., Elvira, J.L.L., and Linthorne, N.P. (2008). Effects of three types of resisted sprint training devices on the kinematics of sprinting at maximum velocity. J. Strength Cond. Res. *22*, 890–897.
69. Miyashiro, K., Nagahara, R., Yamamoto, K., and Nishijima, T. (2019). Kinematics of maximal speed sprinting with different running speed, leg length, and step characteristics. Front. Sports Act. Living *1*, 37. https://doi.org/10.3389/fspor.2019.00037.
70. Hamilton, N. (1993). Changes in sprint stride kinematics with age in Master's athletes. J. Appl. Biomech. *9*, 15–26.
71. Bezodis, I.N., Kerwin, D.G., and Salo, A.I.T. (2008). Lower-limb mechanics during the support phase of maximum-velocity sprint running. Med. Sci. Sports Exerc. *40*, 707–715.
72. Haralabidis, N., Serrancolí, G., Colyer, S., Bezodis, I., Salo, A., and Cazzola, D. (2021). Three-dimensional data-tracking simulations of sprinting using a direct collocation optimal control approach. PeerJ *9*, e10975.
73. Morin, J.B., Edouard, P., and Samozino, P. (2011). Technical ability of force application as a determinant factor of spring performance. Med. Sci. Sports Exer. *43*, 1680–1688.
74. Novacheck, T.F. (1998). The biomechanics of running. Gait Posture *7*, 77–95.
75. Milks, A., Lehmann, J., Leder, D., Sietz, M., Koddenberg, T., Böhner, U., Wachtendorf, V., and Terberger, T. (2023). A double-pointed wooden throwing stick from Schöningen, Germany: Results and new insights from a multianalytical study. PLoS One *18*, e0287719.

STAR★METHODS

KEY RESOURCES TABLE

REAGENT or RESOURCE	SOURCE	IDENTIFER
Deposited data		
Human MRI, bone geometries and muscle data	Charles et al.[32]	https://datacat.liverpool.ac.uk/1536/
Chimpanzee CT bone geometries	Sellers et al.[47]	https://www.frontiersin.org/articles/10.3389/fevo.2022.954838/full#supplementary-material
Gorilla CT bone geometries	Primate Research Institute, Kyoto University, PRICT No. 293 & 294	http://dmm.pri.kyoto-u.ac.jp/dmm/WebGallery/index.html
Orangutan CT bone geometries	Püschel and Sellers[48]	N/A
Bonobo CT bone geometries	Püschel and Sellers[48]	N/A
Gibbon CT bone geometries	Primate Research Institute, Kyoto University, PRICT No. 182	http://dmm.pri.kyoto-u.ac.jp/dmm/WebGallery/index.html
Human and *Au. afarensis* MDA models	This paper	https://doi.org/10.17638/datacat.liverpool.ac.uk/2831
Software and algorithms		
GaitSym software	N/A	http://github.com/wol101

EXPERIMENTAL MODEL AND STUDY PARTICIPANT DETAILS

This study constructed multi-body dynamics computer models of a human and *Au. afarensis*. For the human model, we modified an existing subject-specific musculoskeletal model ('Subject1' in Charles et al.[32]) from previous work.[32] For the *Au. afarensis* model, we constructed a new musculoskeletal model using the 3D digital skeleton from Brassey et al.[49]

METHOD DETAILS

Predicting muscle mass in *Australopithecus afarensis*

Modern humans have a higher proportion of their body mass as lower limb muscle than non-human apes[50–52] (Figure S1). Previous muscle reconstructions of *Au. afarensis* have either assumed proportions that are human,[16] tested human, chimpanzee and/or intermediate masses[7,8,15] or have used manual sculpting to generate predicted muscle masses.[14] As a starting point for testing a range of muscle masses in our running simulations, we developed a new approach, similar to one recently applied to dinosaurs,[53] which derives estimates of the masses of individual muscles or muscle groups based on metrics associated with the available attachment areas on the skeleton in extant great apes and gibbons (Figures 1A and S1; Table S1). Our goal was to establish predictive relationships between bony attachment areas and the masses of associated muscle(s) that could be applied to predict muscle size based on fossilized skeletons. To produce predictive relationships between muscle mass and bony attachments areas that could be applied to hominid fossils, we examined the correlations between measured muscle masses and various skeletal surface areas on the pelvis, femur, tibia and fibula in extant great apes and gibbons (Figure S1; Table S1) using linear regression. We collated lower limb muscle masses of chimpanzees (*Pan troglodytes*), bonobos (*Pan paniscus*), gorillas (*Gorilla*), orangutans (*Pongo*) and gibbons (*Hylobates*) from the literature[50–52] and scaled these values to body masses of individuals for which we were able to acquire 3D skeletal models from CT data (see key resources table). For humans we used subject-specific muscle masses and bone geometries from the same 10 individuals from previously published work,[32,33] and then subsequently represented *Homo sapiens* in the regression analysis by average values from these individuals. Previous work has shown that accurately quantifying individual muscle attachment areas is extremely challenging.[53] For the majority of muscles or muscle groups, we therefore examined correlations between muscle mass and gross bone surface areas, such as the whole femoral shaft (Figure S1; Table S1). We log-transformed bone areas and muscle masses and conducted least squares linear regression in PAST 4 (version 4.11). This yielded statistically significant regressions for 14 individual muscles or muscles groups (Table S1) that we applied to predict the masses of muscle and/or muscle groups in *Au. afarensis* based on the AL 288-1 specimen. We did not recover statistically significant relationships between bone surface areas on the shank and the digital flexor muscles (flexor digitorum longus and flexor hallucis longus) and so these were assigned relative muscle masses intermediate (i.e. averaged) between chimpanzees and humans in our musculoskeletal model of *Au. afarensis*. The freely available digital skeletal model of AL 288-1 from Brassey et al.[49] was used to quantify the same bone surface areas in *Au. afarensis*.

Consistent with the immediate nature of AL 288-1 limb and body proportions, this approach suggests that overall lower limb muscle mass (one limb) in *Au. afarensis* was intermediate between chimpanzees (6.2% body mass[30–32]) and humans (9.6% body mass[32,33]) at 8% total body mass (Figure S1. See below for derivation of AL 288-1 body mass). All individual limb muscles and muscle groups are predicted to have higher relative masses than seen in chimpanzees with the exception of the hamstring and vastus groups (Figure S1). The gluteus maximus, iliopsoas and adductor group are intermediate between chimpanzees and humans, while the ankle flexors and triceps surae group muscle groups are predicted to have slightly greater relative masses than modern humans (Figure S1).

Body segment mass and inertial properties in *Australopithecus afarensis*

We used a convex hulling approach[49,54–56] (Figure S2) to estimate body mass in *Au. afarensis* for size-normalized comparisons of muscle mass and body segment inertial parameters for our musculoskeletal model of *Au. afarensis* (Figure 1). Use of the same digital skeleton means our minimal skeletal convex hulls are the same as those from Brassey et al.,[49] but here we used the mammalian segment-specific convex hull expansion exponents of Coatham et al.[54] to generate the final 'expanded' volumetric model. This yielded total body masses of 22.1kg for *Au. afarensis* AL 288-1 (Figure S2), which is slightly higher than the 20.4kg estimated by the simpler homogeneous whole-body expansion of Brassey et al.[49]

Simulating running performance

We constructed musculoskeletal models of *Au. afarensis* AL 288-1 (Figure 1) and a human using the open-source physics simulation package GaitSym[7,8,21–23] (version 2017). This simulator has the facility to generate movement patterns in musculoskeletal models '*de-novo*' without any pre-defined (i.e. measured) gait or performance data, making it ideally suited to estimating maximum performance in extinct animals. This is achieved by setting a performance goal for the model and using a genetic algorithm optimisation method to search for the pattern of muscle activation that performs best according to that performance goal. Previous application of this approach to humans and birds has demonstrated that it can generate maximum running speeds that are consistent with literature values, even when the model anatomy is more simplified than the models used here.[21] Here, both our *Au. afarensis* and human models had seven functional body segments (head+trunk+upper limbs, right and left thighs, shanks, and feet) with hip, knee and ankle joints restricted to pure flexion-extension. The models were therefore three-dimensional in their representation of body segment geometry and mass properties and muscle-tendon unit geometry, but motions were restricted to planar (two-dimensional) rotation in pure flexion-extension. Bramble and Lieberman[2] noted that modern humans possess a number of derived features that enhance stabilization through independent rotations within the trunk during running. Australopithecines lacked at least some of the morphological adaptations that permit these stabilizing motions in humans, retaining for example a relatively broad, chimpanzee-shaped thorax and broad pelvis.[2] In addition, the relatively wide shoulders of modern humans act to increase the counterbalancing moments generated by arm-swinging, while also permitting energy-saving reductions in forearm mass,[2] which is a relatively lower proportion of body mass in our human model than our *Au. afarensis* model. Our models (and to our knowledge, no currently published forward dynamics bipedal models where gaits are generated entirely predictively without prescribed kinematics and/or kinetics) do not include muscle-controlled, mobile, multi-segment torsos and arm segments. Our models therefore do not account for these adaptive functional differences hypothesised to exist between humans and Australopithecines.

We simplified lower limb musculature into nine aggregated muscles (Figure 1). Six of these muscles were uni-articular, with a moment arm for either flexion or extension across the full range of associated joint motion, and three were bi-articular muscles included to represent the action and function of the rectus femoris (i.e. hip flexion and knee extension), the hamstrings (i.e. hip flexion and knee flexion) and the gastrocnemius muscles (i.e. knee flexion and ankle extension). The muscle model used to calculate force generation consists of a standard Minetti and Alexander[57] contraction model that represents concentric and eccentric contractions using empirically determined force-length and force-velocity relationships. The force generated by the contractile units and elastic elements is solved at each time step via a custom implementation of a Hill-style contractile model combined with a metabolic energy cost prediction function.[57] This model uses a nonlinear fit to empirical values of metabolic energy costs for muscular contraction.[58] The muscle model provides a variety of mandatory and optional input definitions for an individual muscle-tendon unit, depending on the desired complexity with which activation dynamics and force generation are to be represented. Here, because the physiology of extinct animals is not fossilised (and highly detailed representations would require additional speculative assumptions and undesirable complexity) we chose the minimal number of inputs parameters, which were physiological cross-sectional area (PCSA), fibre length, tendon length, maximum contraction velocity (Vmax), force per unit area (or maximum isometric stress), an activation constant and values for the passive elasticity of muscle (parallel element) and tendon (serial element) at maximum isometric force. In all iterations of the human and *Au. afarensis* models described below, the physiological cross-sectional areas of the muscles were calculated by dividing muscle volume (derived from muscle mass, see above) by the fibre length (see below). Values for force per unit area were standardised at 300,000Nm^{-2}, and parallel and serial elasticity set to 60% and 6% strain at maximum isometric stress based on values used in previous studies.[7,8,21–23] Vmax was initially set to 8.4 resting length s^{-1} in all simulations but varied as part of our model parameterization exercise (see below).

To derive muscle masses (and ultimately PCSAs) for the human model, we simplified a detailed subject-specific musculoskeletal of a 35-year-old male (body mass 68.4 kg; height 1.76 m; static hip height 0.91 m; BMI 21.95 kgm^{-2}) by retaining the lines of action of nine muscles representative of the above functions and assigning the masses of 30 individual muscles measured through MRI in this participant to our nine aggregated muscle based on their moment arms.[32,33] We mirrored this procedure in our *Au. afarensis* model

but originally assigned muscle masses based on our predictions from bony attachment areas measured on the digital skeleton, which were approximately intermediate between humans and chimpanzees (see above and Figure S1). To bracket likely extreme scenarios for muscle mass in *Au. afarensis* we also produced model iterations where all muscle masses were universally increased and decreased in size until total lower limb muscle mass matched average values for chimpanzees (6.2% body mass in one limb[50–52] and humans (9.6% body mass in one limb[32,33]) (Figure S1). This not only brackets the likely maximum error bound on predicted running performance in *Au. afarensis* related to uncertainty in muscle mass, but also allows us to approximate the magnitude of impact that evolutionary increases in muscle mass to human values had on running mechanics (Figure S1), while retaining the body and limb proportions of *Au. afarensis*. To complement this analysis, we also tested an iteration of the human models where muscle mass was uniformly reduced so that total limb muscle mass was same proportion of body mass as predicted here for *Au. afarensis* (Figure 3).

We took a similar approach to examine the impact of muscle architecture in the triceps surae muscles on running speed and energetics. Because our models include a smaller number of aggregated muscles, we derived muscle fibre and tendon lengths based on a functional scheme that ensured these simplified muscles were capable of generating reasonable forces across a wide range of joint angles. Specifically, fibre and tendon lengths were calculated by measuring the minimum and maximum length of each muscle obtained by moving the joints through their full ranges of motion. The fibre length of each muscle was then calculated as the length change and tendon length as the mean overall length minus the fibre length for each muscle, similar to schemes used in previous simulation studies using models with simplified musculature.[23,59] In the triceps surae muscles (i.e. a uni-articular and a bi-articular ankle extensor in our models) this led to relatively short muscle fibre lengths and long tendon lengths that are qualitatively (and to a great extent quantitatively) similar to the human soleus and gastrocnemius muscles. Qualitative descriptions and quantitative measures of triceps surae architecture in non-human apes vary somewhat and are not easy to reconcile to derive a meaningful representation that can be re-scaled (to account for size differences) and applied to *Au. afarensis*. Payne et al.[50] reported relatively smaller PCSAs and longer fibres in non-human apes than in humans when triceps surae architecture was normalised to body mass (their Tables 3 and 4). These results are qualitatively consistent with the findings of Thorpe et al.[52] who found that, if both were scaled with geometric similarity to 50kg body, humans would have average triceps surae fibre lengths approximately 3 times shorter than chimpanzees, but PCSAs around 5 times larger. Payne et al.[50] also present evidence for exceedingly small or absent external tendons (their Table 4). Although this suggests a reduced capacity for elastic energy storage in the ankle extensors of non-human apes, the ''tendon length'' in a Hill-type muscle model generally represents both ''internal'' and external tendons.[59] Internal tendon and aponeurotic tissue lengths were not reported by Payne et al.,[50] but for instance in their *Pan paniscus* and *Gorilla* specimens, triceps surae fibre lengths ranged between 6-15.5 cm, at a body mass range of 64-130 kg. In *Pan troglodytes*, other workers have suggested triceps surae fibres to be pennate,[60] and the triceps surae in the *P. troglodytes* model of O'Neill et al.[61] included tendon lengths more than twice the fibre lengths to represent this effect.

Given the general uncertainty that surrounds the extrapolation of such parameters to fossil animals of different body size and proportions, we deliberately tested a highly extreme 'non-human ape' triceps surae morphology by generating a model iteration with relatively long fibres, small PCSAs and a short Achilles tendon. Specifically, we set the tendon lengths for the two triceps surae muscles in our models to 9% mean muscle-tendon unit lengths. This assumes that the external tendon measurements reported in Payne et al.[50] represent the only series-elastic tissue. We set fibre lengths in this model iteration as the mean muscle-tendon unit lengths across the full range of knee and ankle flexion-extension minus these tendon lengths. PCSAs were then recalculated using these new fibre lengths. This approach triceps surae muscles that are extreme in terms of their function for relatively low force generation over a large working range, with relatively little capacity for elastic energy recovery even when compared to the *Pan* model described by O'Neill et al.[61] Thus, this model iteration is much more poorly suited for high performance running (and similar locomotor tasks) and therefore represents a deliberately 'pessimistic' reconstruction of *Au. afarensis* triceps surae morphology, in recognition of the high-level of uncertainty present in soft tissue reconstructions based on fossilized osteology alone.

Vmax, related to muscle fibre type, also represents an important determinant of running performance and is thought to vary in human and extant non-human apes.[20,62,63] Relatively few quantitative comparisons have been human and non-human apes have actually been made in these respects, though it has been shown that triceps surae muscles in humans have considerably more slow-twitch muscles fibres, which are expected to more fatigue resistant (and thus enhance endurance running capacity).[20,62,63] Given the absence of exhaustive data, and the inherent uncertainty of contraction velocity in all fossil animals known from only osteological remains, we varied the Vmax of all muscles in *Au. afarensis* model between 6-12 resting length s^{-1} to quantify its impact on running speed and CoT, based on the recommendation of 12 resting length s−1 for fast-twitch and resting length 4.8 s−1 for slow-twitch fibers by Umberger et al.[64] Because Vmax had less impact on running performance than muscle mass in our *Au. afarensis* model, we only varied muscle mass in our parameterisation analysis of the human model.

For each model iteration, we set the optimisation goal as the muscle activation patterns that resulted in the greatest distanced travelled in 5 seconds, using our standard 'gaitmorphing' approach.[7,8,21–23] Because this machine learning approach is stochastic in nature, we ran multiple independent iterations per model until predicted running speed no longer improved with further optimisation runs in each independent iteration.[21–23] We then continued to optimise gaits with cost of transport added as additional optimisation criteria until reduced energy costs could only be achieved by reducing distance travelled.[7,8] These independent simulation iterations, optimised for distance travelled and energy minimisation, are plotted as individual data points in Figure 2C. Foot-ground interactions were modelled using contact spheres ('geoms') placed across the soles of the feet. Ground contact is initiated when contact spheres intersect with an environmental plane, at which point soft-contact interaction is modelled using basic spring-damper

elements according to a basic Coulomb friction coefficient, and spring and damping constants that together specify the stiffness and damping of the foot-ground interaction. Values were set to those used in our previous simulations of primate locomotion.[7,8,21] We calculated the bone stress incurred in our simulations by treating the limb long bones as irregular beams and calculating the mid-shaft loading on the cross-sectional geometries of the AL 288-1 fossil[31] for *Au. afarensis* and subject-specific geometries for the human subject.[32,33] Specifically, the effect of inertial and muscle forces was calculated from the simulations by extracting the reaction forces and moments in fixed joints placed at the midshaft points of the femora and shanks.[23] To size-normalize maximum speeds to account for differences in body size between modern humans and *Au. afarensis* we converted absolute speeds (m/s) to Froude numbers, calculated as speed^2/gravity*leg length.[65] Animations of the fastest running iterations of the *Au. afarensis* models with human-like and non-human ape-like triceps surae architecture with bone surface area derived muscles masses were generated in Blender by applying custom written scripts (by PVB) to the MDA model musculoskeletal geometry and motion paths exported from GaitSym.

QUANTIFICATION AND STATISTICAL ANALYSIS

To examine the accuracy of predicted maximum running speed in our human model we measured maximum sprinting speed in the same human subject upon which the model was based using a Salter ATS speed gun. The subject was asked to sprint as fast as possible across a ~70m all-weather ("3G") football pitch, while an operator stood approximately halfway along the sprint path and slightly adjacent to the direction of travel, facing towards the oncoming subject in five trials and away from subject (towards the direction of travel) in five trials. The speed gun provides a live display of the measured speed and saves the peak speed from any given trial to nearest 1mph. The subject repeated the running exercise (with breaks between trials) until 10 trials were recorded where the peak speed saved by the gun corresponded to the instantaneous value during the trials observed on the display by the operator. Trials where higher peak values were recorded by the device than were observed by operator on the live display were discarded under the assumption that these were anomalous values resulting, for example, from unsteady operation (i.e. minor shaking/deviation) of the gun. The predicted maximum running speed of the model (7.9m/s) fell within these experimental measured speeds of 7.15–8.05 m/s. Gait parameters like stride length, step frequency and peak vertical ground reaction force from the human model also show reasonably good agreement with published values on human sprinting[66–73] (Figure S3). Our model also yielded simulation iterations with CoT values that are consistent with experimentally measured values[2] between 2.8–5.5m/s (Figure 3). However, stance phase joint kinematics show a more variable match to experimental measures[68,69,72,74] (Figures S4A–S4D), which is perhaps not surprising given our simplified muscular anatomy, omission of ligamentous structures and restriction of joint rotations to pure flexion-extension. Torso orientation (anterior-posterior tilt) remains within 5 degrees of experimental values throughout stance, while model hip (Figure S4A) and ankle (Figure S4C) angles replicate the qualitative patterns of joint angle change seen across the stance phase. At the hip, absolute angles are within 10 degrees of measured values in early to mid-stance and fall within the experimental range from mid- to terminal stance (Figure S4B). The ankle remained consistently between 10-20 degrees more plantar flexed throughout stance than experimentally measured values (Figure S4D). However, the match between knee joint angles was much poorer, with the model's knee joint remaining considerably more extended than experimentally measured values throughout most of the stance (Figure 4C). Only in terminal stance did flexion of the model's knee bring it within the experimentally measured range (Figure 4C). Overall, the consistency between simulated and experimentally measured gaits in humans[17,18,75,19,66–69] (Figures 3 and S3; Tables S2 and S4), particularly the 'global' performance parameters that the model was primarily constructed to predict (speed and CoT) provides confidence that our approach can deliver relatively accurate estimates of gross locomotor performance, despite considerable anatomical simplifications to the models (see also Sellers and Manning[21]).